Case Studies in Thermal Engineering 6 (2015) 171–181

Contents lists available at ScienceDirect

Case Studies in Thermal Engineering

journal homepage: www.elsevier.com/locate/csite

Scrutiny of plasma spraying complexities with case study on the optimized conditions toward coating process control

Ridha Djebali [a,*], Bernard Pateyron [b], Mohammed ElGanaoui [c]

[a] ISLAIB – Béja 9000, University of Jendouba, Tunisia
[b] CNRS – SPCTS/CEC 12, Rue Atlantis 87068, Limoges, France
[c] Univ. Lorraine, (LERMAB & GREEN), Longwy Inst. Technology, France

ARTICLE INFO

Article history:
Received 10 July 2015
Received in revised form
8 September 2015
Accepted 13 September 2015
Available online 16 September 2015

Keywords:
Plasma jet
Gas mixture
Operating conditions
Spraying
Coating
Process control
Optimization

ABSTRACT

In the present study, we investigate a PSP using the *Jets&Poudres* soft. The plasma gas understanding is given to highlight the effects of gas mixtures proportions on diffusion parameters. An overview on the process complexities at main subsystems is given with focus on Argon plasma and optimal mixing; the powder acceleration and heat-up modeling are also presented. Under literature conditions and for He–Ar–H_2 65–30–5% gas, it was found that the droplet's primary way is to coat. The used ternary mixture gives superior efficiency compared to the pure Argon which shows a prior way to rebound. Moreover, medium particles ($d_p \approx 45$ μm) present the high deposited rate among the splashed mass, a 100% molten ratio is observed for the small powder and only particles of size below 40.3 μm have evaporated, particles of initial diameter between 40.3 and 49 μm are fully molten and all particles above 71.9 μm are fully solid. The coat formed by the deposited mass will transfer a large amount of heat to the substrate (9–58 MW/m^2). The crushed particle's rate is about 4% from the investigated number and the average fully molten particle's rate is about 72% and the rest of particles arrive in solid sate.

1. Introduction

Coating treatment of surfaces by plasma spraying remains an important manufacturing process which is extensively used in industrial applications to enhance the performance of engineering components such as coating of pistons, piston rings and shafts, and improving resistance to thermal degradation, corrosion and wear.

Besides, the arc PSP is of great complexity due to the various parameters involved in three levels [1–5]. First, the generation of the plasma arc into the torch (nozzle diameter, current *I*, voltage *U*).

Second, we cite the plasma jet flow in interaction with the powder material jet, where the plasma jet parameters (composition, enthalpy, temperature, velocity, viscosity and thermal conductivity, etc.) are highly variable, the jet length and the air engulfment in the jet enhancing turbulence. Others parameters are related to the powder-injector (internal diameter, position, tilting angle, carrier gas: composition and feed rate, etc.), adding the parameters related to the powder itself (material morphology, shape, size, residence time in the jet, etc.). In a third level, the parameters correspond to the coat formation (materials properties, substrate preparation, spraying distance, relative movement torch/target, incidence tilt, substrate cooling, residual stresses, etc.) and eventually the variability of the above-mentioned parameters (dispersion). The various cited parameters make the plasma spraying a multi-complexity problem.

* Corresponding author.
E-mail addresses: ridha.djebali@ipein.rnu.tn, jbelii_r@hotmail.fr (R. Djebali).

http://dx.doi.org/10.1016/j.csite.2015.09.005

Nomenclature

Vector quantities

$\vec{u}_g$	gas velocity (m/s)
$\vec{u}_p$	particle velocity (m/s)
$\vec{x}_p$	particle position (m)
$\vec{F}_d$	drag force (N)
$\vec{F}_g$	gravity force (N)
$\vec{F}_{ma}$	force due to additive mass (N)
$\vec{F}_{th}$	thermophoretic force (N)
$\vec{g}$	gravitational field (=9.81 m/s²)

Physical parameters

a	thermal accommodation coefficient
A_p	particle surface, $=\pi {d_p}^2$
C_D	drag coefficient
C_{pp}	particle specific heat (J/mol K)
d_{inj}	injector diameter (m)
d_p	particle diameter (m)
f_{kn}	corrective factor related to Knudsen effect
f_{prop}	corrective factor related to boundary layer effect
h_f	convective heat transfer coefficient (W/m²/K)
Kn^*	Knudsen number
k_p	particle conductivity (W/m²/K)
L_e	material latent heat of boiling (J/kg)
L_m	material latent heat of melting (J/kg)
m_p	Liquid–solid averaged particle mass (kg)
N_f	modified Nusselt number
Pr_w	Prandtl number of hot gas at *Tw*
Q_{conv}	convective heat flux received by the particle (W/m²)
Q_{net}	total heat flux received by the particle (W/m²)
Q_{rad}	radiative heat flux received by the particle (W/m²)
Re	relative Reynolds number, $\nu_g d_p/\lvert\vec{u}_g-\vec{u}_p\rvert$
Re_p	particle Reynolds number, $=\rho_p d_p u_p/\mu_p$
t	particle time (s)
T	physical gas temperature (K)
T_∞	local jet temperature (K)
T_a	ambient temperature, 300 K
T_e	material boiling point (K)
T_m	material melting point (K)
T_p	particle temperature, $=T_p(t, r)$
T_w	particle–wall temperature
X_p	volumetric melt fraction of the particle
ρ_g	gas density: volumetric mass (kg/m³)
ρ_p	particle density (kg/m³)
μ_g	gas dynamic viscosity (kg/m/s)
γ	specific heat ratio

Subscripts, superscripts and abbreviations

b	boiling
g	gas
ma	additive mass
p	particle
$prop$	gas property
th	thermophoresis
w	wall
FD	Finite Differences
LTE	Local Thermal Equilibrium
ODE	Ordinary Differential Equations
PSP	Plasma Spraying Process
∞	far from particle
$\dot{m}$	rate of mass vaporization
min	minimum value
max	maximum value
av	average value

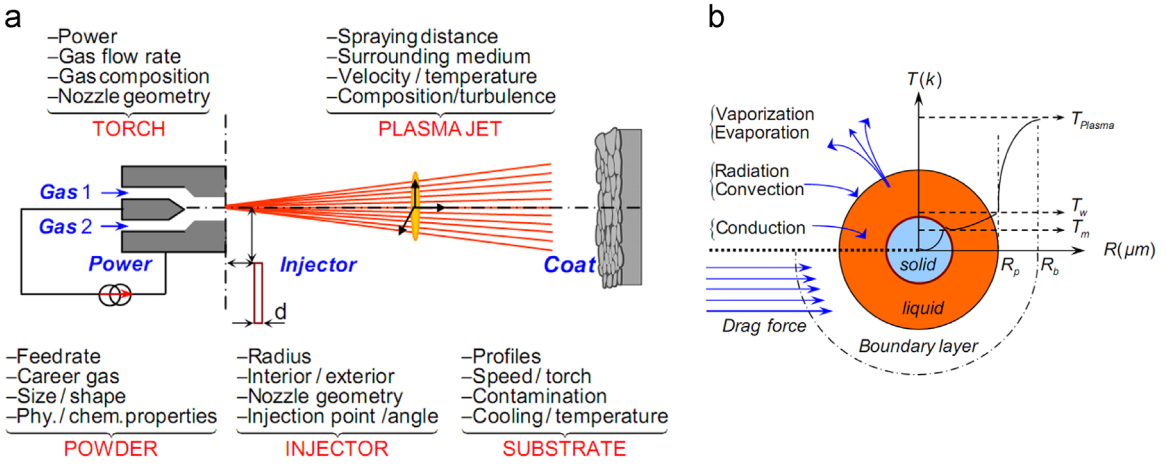

Fig. 1. Sketch of the plasma spraying principle and complexities. (a) The DC plasma torch, the plasma jet, the powder injector, the substrate and the coat formation. (b) Zoomed view of particle momentum, heat and mass transfer phenomena occurring in its surrounding boundary layers.

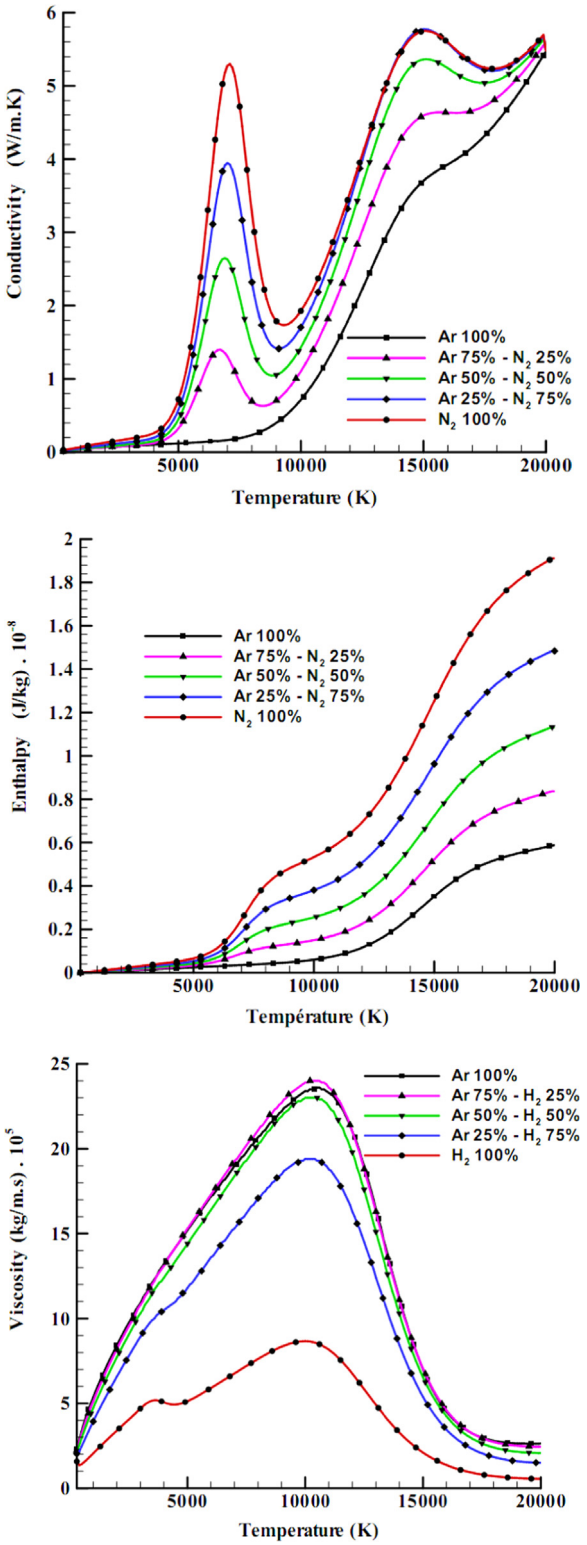

Fig. 2. Effects of proportions in plasma gas mixtures on the thermal conductivity (top), the specific enthalpy (middle) and the dynamic viscosity (bottom) variations in the temperature range 0–20,000 K.

The process is also a source of experimental and numerical works [1–8] to achieve high performance and reduced experimental efforts. In the following sections, an overview on plasma gas and optimal mixing will be presented, the powder acceleration and heat-up modeling will be given. We will finally investigate a PSP case using the code *Jets&Poudres*

under carefully chosen conditions consistent with that recommended by Djebali et al. [1].

2. Plasma gas understanding

2.1. Process complexities at various levels

The PSP complexity has met with particular interest in former studies. Vardelle et al. [9] have in part conducted a work on spray parameters and particle behavior relationships during its sojourn in the hot plasma gas. The discussed elements are: the particle injection (injection momentum, powder injector tilting), the particle size and morphology, the spraying parameters and torch design (power level, Hydrogen percentage in Argon, plasma gas flow rate).

The authors work addressed also a comparison of Ar–H_2 and Ar–He mixtures and explore the nozzle diameter surrounding atmosphere effects. The author's work emphasized through flux measurements the importance of the carrier gas flow rate that must be adjusted to the plasma jet momentum depending on some parameters such as in particular gas nature, which is in accordance with the conclusions drawn by Djebali et al. [1] stating that the primary gas flow rate has the second key role in particle arrival state.

In Fig. 1, one can note the huge complexity of the process at different levels related mainly to the characteristics of the torch, the powder, the injector, the plasma jet and the substrate. Even further, a particle flying in the hot gas undergoes a very complicated momentum, heat and mass transfer phenomena occurring in its surrounding boundary layers.

In the following, we will focus mainly on the effects of plasma gas nature on the arrival characteristics of sprayed powder.

2.2. Which plasma gas for which application?

For diatomic or polyatomic gases, much energy (enthalpy) is required for the dissociation (N_2, H_2, NH_3, CH_4, etc.) which increases the specific enthalpy and thus the voltage need in the plasma torch. Besides, due to the dissociation and ionization, the number of moles of gas varies with the temperature and therefore the atomic masses (and atomicity). Thus, a diatomic gas at 300 K is monoatomic beyond the dissociation temperature. Virtually, H_2 is not used as pure (for lack of mass), that is why Argon is generally added; and it is the same with Helium gas. For Nitrogen (N_2), it is typically used as pure and hydrogen or Helium may be added. Then, optimal ternary mixtures currently appear to be of type Ar–He–H_2.

The dissociation and ionization phenomena cause huge variations in thermal conductivity. The Nitrogen and hydrogen are added to increase the heat transfer in the vicinities of the dissociation temperatures near 3500 K for H_2 and 7500 K for N_2. For H_2, with a lower dissociation temperature, it is the most widely used gas in a point of view of heat transfer. Helium gas has a much higher thermal conductivity; its ionization begins at 16,000 K. Helium gas improves the impact of the particles by increasing the viscosity of the gas mixture beyond 10,000 K and limiting the phenomena of turbulence in vicinities of the arc column (Fig. 2).

In Fig. 1 (top) one can see the effect of the adding Nitrogen on the conductivity of the mixture. At around 7500 K, we note the appearance of peaks of Nitrogen dissociation resulting in an increase of the thermal conductivity of the mixture at a rate of 1.3 W/mK for each addition of 25% Nitrogen. At peaks, the conductivity of pure Nitrogen is four times greater than that of the Ar–N_2 mixture (75–25% vol.) and 30 times that of the pure Argon. The conductivity of Nitrogen is 5 times greater than that of pure Argon near 9000 K; then, as the temperature increases gradually both conductivities increase and another peak appears for Nitrogen, beyond which (near 20,000 K) both conductivities tend towards one another. The calculations are done by the help of the T&Twinner soft [10].

In arc plasma spraying, when the percentage of Nitrogen increases, the thermal conductivity of the plasma gas increases and the arc is constricted. This leads to increasing the electric field and the arc length which results in a better energy dissipation and greater expansion of the jet with high flow velocities. Fig. 1 (middle) shows the specific enthalpy variation vs temperature for the Ar and N_2 pure gases and their mixtures Ar–N_2 at atmospheric pressure.

We note here, that as far as the percentage of Nitrogen increases, there is a significant increase (almost linearly with the rate of Nitrogen addition) in the specific enthalpy of the Ar–N_2 mixture. This augmentation was noticed in the vicinity of dissociation peaks near 7500 K and 20,000 K. However, beyond 10,000 K, a strong variation of the plasma specific enthalpy (Ar–N_2 to N_2 as example) causes increase in flow velocity instead of the temperature because of large variation of enthalpy with a small increase in temperature.

Besides, the addition of Nitrogen to the Argon has no significant effect on the viscosity of the mixture. The viscosity of the Ar–H_2 mixture does not differ from that of pure Argon for the proportion of H_2 up to 50%. Once the rate of Argon is less than 25%, the viscosity of the mixture drops sharply as shown in Fig. (1) (bottom). Therefore, a couple Ar–H_2 improves the jet driving due to the heavy Argon and increases the plasma jet velocity at high temperatures.

2.3. Argon plasma and optimal mixing – an overview

The most used plasma spraying gas is Argon. It has better thermophysical properties; it has the advantage of being inert [11] and also it has low ionization temperatures so low enthalpies of use of the torch. Its thermal conductivity is lower, therefore cooling losses are less important, and this is a reason why Argon is used for initiating the arc and also why plasma

torches are more stable (no erosion) with Argon. Moreover, due to its density, Argon has the property of being heavy (as described above) which allows a good particle transport in flight. More preferably, it should be noted that the particle's residence time in a plasma torch of conventional DC arc is about 0.5–1 ms; and an induction torch where the flow velocity is from 20 to 30 times lower, the residence time is of the order of 5–25 ms, which explains the possibility to melt much larger than plasma arc particles using a low thermal conductivity gas such as Argon. It is worth to mention here that the plasma spraying exists in two modes, the so-called plasma Direct Current (DC) which interests us in the following and Radio Frequency (RF) inductive plasma which differs from the first just in the velocity range (<50 m/s) and gas temperature ($\sim$8000 K) (see Dresvin and Mikhailov [12]).

These thermophysical characteristics distinguish Argon to be the primary gas in plasma spraying. The improvement of the Argon plasma can be accomplished by addition of other gases such as Hydrogen, which in turn, is considered as an ideal secondary gas to increase the enthalpy and thermal conductivity of the plasma without much changing its temperature.

The enthalpies of Helium and hydrogen are highly superior to that of Argon. However, beyond 10,000 K viscosity of ternary mixture H_2–Ar–He becomes significantly higher than that of the Ar–H_2 mixture. This, according to Fauchais et al. [13], reduces the training of the ambient air by the plasma jet and extends the plasma jet. Furthermore, the plasma jet core of the mixture H_2–Ar–He remains laminar as the Ar–H_2 mixture. The air is driven further from the outlet of the torch (nozzle) of about 30 mm (instead of 10 mm for a plasma of binary mixture Ar–H_2), which allows a better heat exchange with the particles flying in this zone. For the ternary mixture Ar–H_2–He, primarily the augmentation of hydrogen rate increases the specific enthalpy. This ternary mixture is considered as an optimal mixture in plasma spraying; the percentages of the various components depend essentially on the intended application.

3. Powder acceleration and heat-up modeling

For the particles in-flight in a plasma jet the two characteristics studied are the motion (trajectory, velocity, acceleration) and the thermal evolution (temperature, physical state, heat flux) [10].

3.1. Particles acceleration

A particle moving in a plasma jet is subjected to few forces. The particle's motion equations are expressed as

$$\frac{\partial \vec{x}_p}{\partial t} = \vec{u}_p \text{ and } m_p \frac{\partial \vec{u}_p}{\partial t} = \vec{F}_d + \vec{F}_g + \vec{F}_{ma} + \vec{F}_{th} \tag{1}$$

The most important force acting on the particle is the drift force (drag force). When a particle and a fluid (here plasma) are in relative motion, a drift force is given by the fluid to the particle. This force comes from current lines' dissymmetry between particle upstream and downstream. This force is defined as

$$\vec{F}_d = -C_D \frac{\pi \rho_g d_p^2}{8} |\vec{u}_g - \vec{u}_p| \left(\vec{u}_g - \vec{u}_p\right) \tag{2}$$

The drift coefficient C_D depends on the morphology of the particle and the Reynolds number. Note that the drag force is the more influent on particle trajectory and acceleration.

The modified drag coefficient C_D is defined as [14]

$$C_D = \left(\frac{24}{Re} + \frac{6}{1 + Re^{1/2}} + 0.4\right) f_{prop}^{-0.45} f_{kn}^{0.45} \tag{3}$$

where f_{prop} and f_{kn} are additional correction factors [14,15] accounting for strongly varying plasma properties and Knudsen non-continuum effects in the boundary layers where the temperature of the hot gas flowing over a particle/droplet drops drastically (Fig. 1), and is defined as follows [14–16]:

$$f_{prop} = \frac{(\rho\mu)_\infty}{(\rho\mu)_w} \text{ and } f_{kn} = \left(1 + \frac{2-a}{a} \frac{\gamma}{1+\gamma} \frac{4}{Pr_w} Kn^*\right)^{-1} \tag{4}$$

The gravity force is given by

$$\vec{F}_g = -\frac{\pi}{6} d_p^3 \left(\rho_p - \rho_g\right) \vec{g} \tag{5}$$

The additive weight force (due to additive mass) is engendered by particle moved volume of fluid. IT is defined as

$$\vec{F}_{ma} = -\frac{\pi}{6} \rho_g d_p^3 \frac{\partial \vec{u}_g}{\partial t} \tag{6}$$

The force of thermophoresis is linked to important temperature variation around the particle. This force pushes the particle from hot areas to cold areas. The corresponding expression was earlier developed by Derjaguin and Bakanov in 1959 and by Waldmann and Schmitt in 1964 [17]. The thermophoretic force is then written in the free molecular regime ($d_p < \lambda$) in a temperature gradient as follows:

$$\vec{F}_{th} = \frac{-p\lambda\, d_p^2\, \vec{\nabla T}}{T} \tag{7}$$

and in the continuum regime ($d_p > \lambda$) as the following formula proposed by Talbot and co-workers [18] over the entire range $0 \le Kn = 2\lambda/d_p \le \infty$which agrees within 20% or better with most available experimental data. The Talbot expression is given by

$$\vec{F}_{th} = \frac{-9\pi\mu^2 d_p \xi\, \vec{\nabla T}}{2\rho_g T} \tag{8}$$

$$\xi = 2C_s \frac{(k_g/k_p + C_t Kn)}{(1 + 3C_m Kn)(1 + 2k_g/k_p + 2C_t Kn)} \tag{9}$$

$Kn = d_p/\lambda$, C_s=1.147, C_t=2.20 and C_m=1.146, and λ is the mean free path, k_g and k_p are the thermal conductivity of the gas and the particle respectively.

Other forces intercede in the trajectory of the particle expression but are not considered here such as force due to the particle rotation, the pressure gradient force and the history force of Basset that intercede when boundary layer around the particle varies very quickly (i.e. wakes of bubbles in fluidized bed); this force is insignificant under plasma spray conditions.

3.2. Thermal treatment of particles

The thermal treatment of particles during its sojourn in the plasma jet follows four sequences [10,14,16] as follows.

3.2.1 Solid particle heating

Particle temperature (T_p) is calculated with a thermal assessment in its rounding boundary layer. A reduced expression of this assessment is given by

$$\frac{\partial T_p}{\partial t} = \frac{6Q_{net}}{\pi d_p^3 \rho_p C_{pp}},\ T_p \ne (T_m, T_e) \tag{10}$$

with Q_{net} being the thermal flux received by the particle by conduction and convection.

3.2.2 Melting at constant temperature $T_p = T_m$

The particle injected initially at ambient temperature, heats-up until $T_p = T_m$, say the melting point. Here, we consider the heat received by the particle is entirely converted into latent heat of melting L_m. The part X_p of melting mass grows according to the expression

$$\frac{\partial X_p}{\partial t} = \frac{6Q_{net}}{\pi d_p^3 \rho_p L_m},\ T_p = T_m \tag{11}$$

The fraction X_p ranges between 0 and 1, so the particle is solid for X_p=0 and is completely molten for X_p=1.

3.2.3. Liquid particle heating

At this step, there are two possibilities: the particle liquid phase vaporizes or does not vaporize. If vaporization is not assumed, heating of the particle state follows a heat-up expressed by Eq. (10) until reaching the boiling temperature T_e. However, if vaporization of the liquid phase is assumed, particle diameter follows the expression as

$$\frac{\partial d_p}{\partial t} = -\frac{2Q_{net}}{\pi d_p^2 \rho_p L_e},\ T_p = T_e \tag{12}$$

where $Q_{net}/L_e = \dot{m}$.

Assuming the particle-temperature is uniform within the particle, its heat-up can be described by solving the heat transfer balance equation by convection Q_{conv} and radiation loss Q_{rad} at the particle surface. The heat amount Q_{net} exchanged between the particle and its surrounding is defined as $Q_{net} = Q_{conv} - Q_{rad}$, where $Q_{conv} = A_p h_f (T_\infty - T_w)$ and $Q_{rad} = A_p \varepsilon\sigma (T_w^4 - T_a^4)$, and the particle temperature T_p is estimated in the surrounding boundary layer. The convection heat transfer coefficient h_f is estimated from the semi-empirical Ranz–Marshall-type correlations in terms of the modified

Nusselt number, Nu_f

$$h_f = Nu_f \lambda_p / d_p \tag{13}$$

where Nu_f is obtained from the particle Reynolds number as

$$Nu_f = (2 + 0.514 Re^{1/2} Pr^{1/3}) f_{prop}^{0.6} f_{kn} \tag{14}$$

3.2.4Vaporization at constant temperature $T_P = T_b$

Reaching the boiling temperature ($T_p = T_b$), the heat flux received by the particle is entirely converted into latent heat of vaporization. The time history of the particle diameter is governed by the same relation of Eq. (12).

4. Numerical method

4.1. The Jets&Poudres code overview

The GENeral MIXing (GENMIX) computer code has been developed by Spalding and Patankar [19] to solve 2D parabolic ODE by FD method and was known as the Bikini method because it requires a very low-cost memory and computing time. GENMIX code simulates steady flows predominantly in one direction, without recirculation or diffusion effects in that direction and in LTE. The clever software embodies a self-adaptive computational grid, which enlarges or contracts to cover only the regions of interest, which explains the small need of computing time (less than two seconds of plasma jet computing).

The fast software *Jets&Poudres* [10] was built on the GENMIX code and upgraded by using thermodynamic and transport properties closely related to the local temperature and composition of the plasma. These properties are obtained from T&TWinner database [10]. The *Jets&Poudres* code simulates laminar and turbulent plasma jet flows using the classical mixing length which appears to be the simplest and fastest.

4.2. The Jets&Poudres settings

The models of PSP implemented in the *Jets&Poudres* software take into account the spray instance (combustion flame or standard plasma gun) with parameters related to power and gun. The program allows calculating many jets fields such as temperature, pressures and velocity and determines the dynamic and thermal history in each point for single particle; it allows assessing if the in-flight particle was partially/completely melted, the percent of molten material used subsequently to investigate the coat formation or the splat morphology [20].

The model *Jets&Poudres* forecasts the dynamic [21] of a single or multi particles fed in a plasma jet. Its aim is not to forecast a result very close to experiment but to compute rapidly the parameters of the plasma spray, to present synthetic and explicit results and to give the tendencies and phenomena orders of magnitude.

4.3. Code credibility

Even the *Jets&Poudres* code was extensively used and validated on cases of plasma gases, operating conditions and

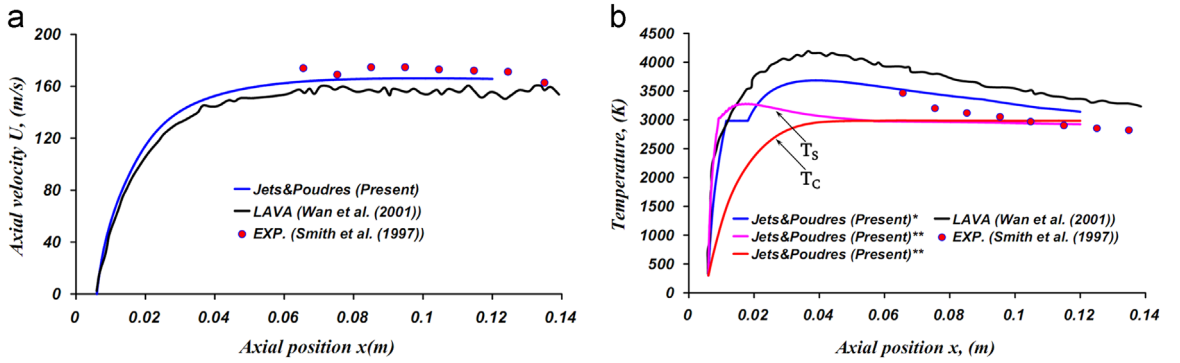

Fig. 3. Axial velocity and temperature of sprayed ZrO_2 particle vs axial distance. LAVA [22] softwares predictions and experimental data of Smith et al. [23] are plotted as references. (*) for thin model is used and (**) for thick model.

spraying conditions and have compared very well experimental and many CFD codes such as ESTET-3.4 (see [21]). We conduct here a plasma spraying case on ZrO_2 particle injected in Ar–H_2 plasma. The results of our model are compared to the predictions of the code LAVA (Wan et al. [22]) and the measurements of Smith et al. [23]. The thick and thin models (with/without conduction phenomena inside the particle) of the software *Jets&Poudres* are considered in this comparison. The injection point is located at (6 mm, −8 mm) away from the nozzle exit. The argon carrier gas flow rate is 1.1 L/min, resulting in a mean velocity of 15 m/s at the injector exit. The particle velocity (Fig. 3a) and particle temperature (Fig. 3b) obtained by the present model show quite good agreement with measurements and predictions of LAVA [22] softwares for both the thin and thick models. This can give a certain confidence in the following results of the model.

5. Case study results and discussions

In the present case study, the plasma jet and the PSP are simulated by the help of the soft *Jets&Poudres*. The plasma jet conditions are: the primary gas is the ternary mixture He–Ar–H_2 65–30–5%, the nozzle radius is 4 mm, the gas flow is 30 NL/min, the spray distance is 10 cm as conventionally used, and the electric power is 17.5 kW (efficiency $\eta=52\%$). The plasma is issuing into the atmospheric air. The present conditions result in a maximum nozzle exit velocity of 523 m/s and a maximum temperature equal to 12,000 K. The turbulence is handled using the alternate modified mixing length. The spraying conditions are: the injector diameter is 1.8 mm, the powder material is the dense Zirconia (ZrO_2) in a Gaussian distribution (with min-size=35 μm, av-size=50.7 μm, max-size=73.9 μm and a standard deviation sd=10.4 μm, ie a total mass of 2.91×10^{-7} kg) and injected to a velocity of 7.4 m/s (career gas feed=1.13 NL/min) and to a half-cone angle of 7°. The granulometry percentage occurrence is sketched in Fig. 4. The injector is fixed at (4.5 mm, −7 mm) away from the torch exit. The present plasma jet and spraying conditions are chosen to be in conformity with the conclusions drawn in our past work using Taguchi experimental design under H_2–Ar 75%. A sketch of the plasma jet temperature field and the powder spray jet is presented in Fig. 5. Table 1 lists some characteristics of the particles states when impacting the target screen.

From Fig. 5, one can see that the spray jet is slightly inclined from the symmetric axis to a solid angle of $\sim\arctan(u_{r\text{-}av}/u_{z\text{-}av})\approx 1.8°$. This result agrees slightly with the range recommended by earlier works [9] stating that an optimum trajectory is an angle of 3–4° relative to the torch axis to allow good coating of the molten particles and avoid normal incidence that causes splashing phenomena. This indicates that the chosen values may be of practical interest.

The general analysis of the present spray by *Jets&Poudres* indicates that from the 700 particles, 628 are in jet and the 72 others have vaporized; resulting in 95.96% of treated mass and 4.04% of mass out jet. This reveals, primarily, that the jet and the spray conditions let spraying process with superior efficiency.

Fig. 6 shows the dots of particles flattening on a substrate screen. The major of the sprayed powder are deposited symmetrically to the vertical plan ($x=0$) and the normalized deposited height diminishes with increasing the ordinate y (Fig. 7a). As one can see, also, in Fig. 7b, the heavy (large sizes) particles/droplets across the hot gas are to be on top of the spray jet; however, the small size particles/droplets are driven by the jet current to be in the bottom of the powder spray jet.

Besides, during its in-flights the heavy particles are away from the plasma jet center-line where hot gas, then, will not acquire the sufficient heat to melt. The particles arrive and hit the substrate in solid state, and then they are rebound as depicted in Fig. 7c: the only rebounding particles are red in the top-right side of the substrate. These particles are in blue in

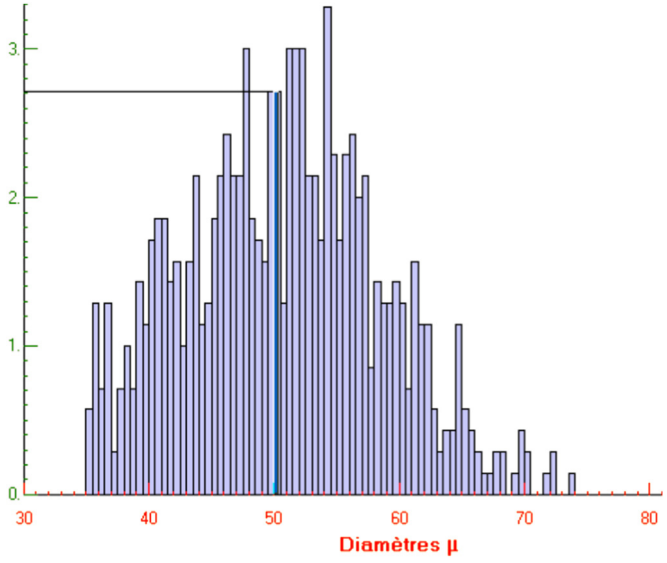

Fig. 4. Particles size percentages occurrence.

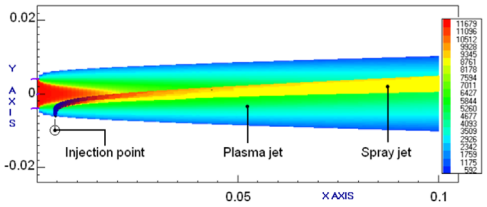

Fig. 5. Color maps of the plasma jet temperature distribution with fringes legend and the spray jet simulated using *Jets&Poudres*. (For interpretation of the references to color in this figure legend, the reader is referred to the web version of this article.)

Table 1
Some characteristics of the impacting particles. (*) Means the initial diameter for the impacting particles.

Impact property	Min	Av.	Max
Axial velocity u_z (m/s)	87.3	125.0	148.0
Deposited height (μm)	0.6	–	1
Initial diameter (μm)$^{(*)}$	40.3	52.2	73.9
K-Sommerfeld	0	912	1160
Molten ratio (%)	0	71.8	100
Particle Reynolds number	0.62	1.73	1.98
Powder mass (%)	0.067	0.153	0.413
Radial position (mm)	0.77	2.28	4.75
Radial velocity u_r (m/s)	3.00	3.91	4.73
Rebound mass (%)	0	0.002	0.413
Residence time (ms)	1.37	1.53	1.88
Splash deposited mass (%)	0.067	0.150	0.355
Splashing ratio	0	8.63	10
Surface flux (MW/m^2)	8.77	40.60	58.40
Temperature (K)	2850	3120	4630

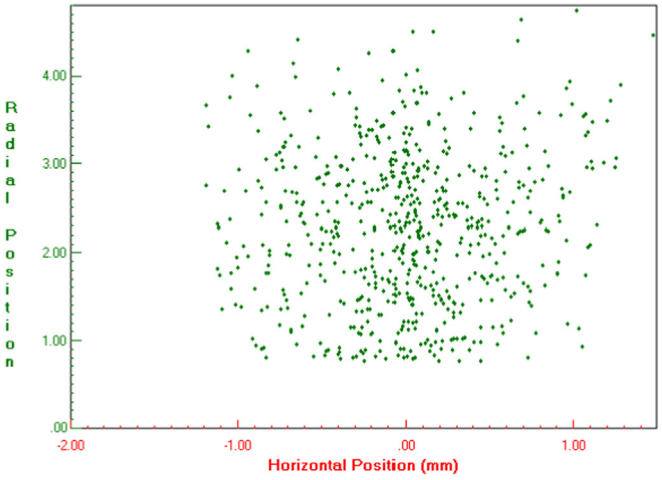

Fig. 6. Points cloud of particles impacting the target screen at 10 cm of spraying distance.

Fig. 7d, because they rebound in solid state (no splashing phenomena). The average plash deposited mass is 0.15%, and by multiplying by 628 (in jet particles) gives 94.2% which is close to the treated in jet mass given here-above.

Even more, some heavy particles present the high deposited rate among the splashed mass (Fig. 7d); this is certainly due to its impacting state which is semi-molten state. Besides, a 100% molten ratio is observed for the small powder in Fig. 7e ($d_p \leq 49$ μm) which, due to its low weight, is driven parallel and near the plasma jet centerline where hot gas acts; which agrees with the former findings [9] that only the particles below 45 μm in diameter are fully molten.

In the present case study, particles of size below 40.3 μm have evaporated, particles of initial diameter between 40.3 and 49 μm are fully molten and all particles above 71.9 μm are fully solid, and the connection is quasi-linear for the semi-molten droplets. One can remark, also, that as the melting ratio decreases coordinates increase radially; this is because at the jet edge, the gas is cold and does not allow particles to melt. It is good to mention, also, that the molten state and velocity of particles upon impact on the substrate control their flattening and the cooling of the resulting splats and then influences absolutely the thermo-mechanical properties of the coatings.

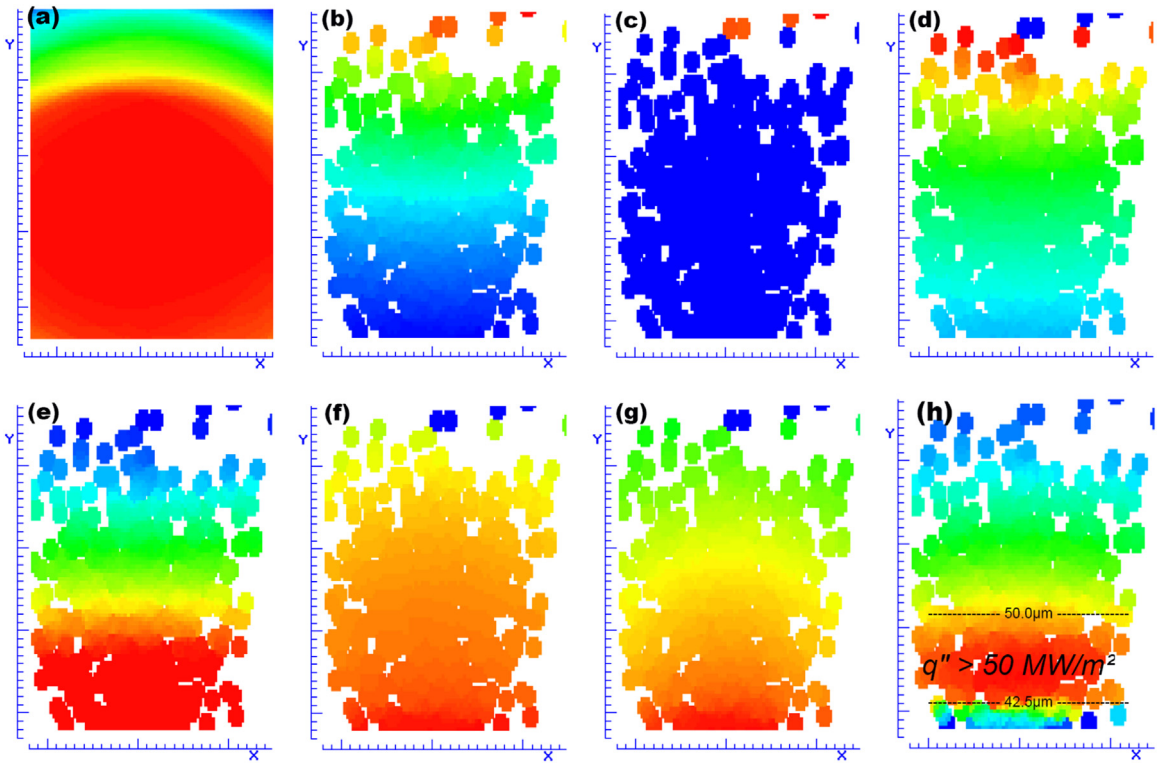

Fig. 7. Color maps of normalized deposited height (a), powder mass (b), rebound mass (c), splash deposited mass (d), molten ratio (e), splashing ratio (f), Sommerfeld number (g), surface flux (h). Blue: min values and red: max values. (For interpretation of the references to color in this figure legend, the reader is referred to the web version of this article.)

Due to the high melting ratio and the trajectory near the jet centerline with high axial velocities, the driven droplets are subjected to the splashing phenomena which is accented in the impact region of small-to-medium particles (Fig. 7f). The splashing phenomenon is assessed by the help of the *K*-Sommerfeld number, which in turn marks its high values in the impact region of small-to-medium particles (Fig. 7g). The general trend indicates a prior way to coat. Furthermore, the coat formed by the deposited mass will transfer a large amount of heat to the substrate in the range (8.77–58.40) MW/m^2, its majority ($>$ 50 MW/m^2) is provided by particles of size ranging from 42.5 to 50.0 μm.

6. Concluding remarks

As the Ar–He–H_2 mixture presents some advantage over pure Argon and Ar–H_2 mixture, the present work falls into this topic and aims to investigate PSP under chosen conditions seeking for the optimization of plasma spraying parameters toward coating process control. The following can be concluded from this study.

The Ar–He–H_2 coating shows superior efficiency compared to the pure Argon gas which shows a prior way to rebound and an average molten ration of about 6.6% under the same spraying conditions.

Medium particles ($d_p \approx 45$ μm) present the high deposited rate among the splashed mass.

A 100% molten ratio is observed for the small powder and only particles of size below 40.3 μm have evaporated, particles of initial diameter between 40.3 and 49 μm are fully molten and all particles above 71.9 μm are fully solid.

The crushed particle's rate is about 4% from the investigated number, the average fully molten particle's rate is about 72% and the rest of particles arrive in solid sate.

The coat formed by the deposited mass will transfer to the substrate a maximum heat amount of 5.8×10^7 W/m^2.

We hope this study will provide useful informations on the spraying process toward control of the coating formation.

References

[1] R. Djebali, M. Toujani, B. Pateyron, Taguching the atmospheric plasma spraying process: influence of processing factors on droplet impact properties obtained on dense ZrO_2 and H_2Ar75% plasma gas, Comput., Mater. Contin. 37 (3) (2013) 147–160.

[2] R. Djebali, B. Pateyron, M. El Ganaoui, A lattice Boltzmann based investigation of powder in-flight characteristics during APS process, Part II: effects of

parameter dispersions at powder injection, Surf. Coat. Technol. 220 (2013) 157–163.
[3] A. Arcondéguy, G. Gasgnier, G. Montavon, B. Pateyron, A. Denoirjean, A. Grimaud, C. Huguet, Effects of spraying parameters onto flame-sprayed glaze coating structures, Surf. Coat. Technol. 202 (2008) 4444–4448.
[4] W.L.T. Chen, J. Heberlein, E. Pfender, B. Pateyron, G. Delluc, M.F. Elchinger, P. Fauchais, Thermodynamic and transport properties of argon/helium plasmas at atmospheric pressure, Plasma Chem. Plasma Process. 15 (3) (1995) 559–579.
[5] F. BenEttouil, B. Pateyron, H. Ageorges, M. El Ganaoui, P. Fauchais, O. Mazhorova, Fast modeling of phase changes in a particle injected within a d.c plasma jet, J. Therm. Spray Technol. 16 (5–6) (2007) 744–750.
[6] Y. Yu, J. Xu, N. Gan, Effects of parameters on continuously working plasma synthetic jet, Eng. Appl. Comput. Fluid Mech. 8 (1) (2014) 55–69.
[7] L. Feng, W. Long, W. Feng, Research on match of swirl-chamber and conical spray in indirect injection engine, Eng. Appl. Comput. Fluid Mech. 7 (2) (2013) 272–281.
[8] L. Ma, W.J. Lv, Q. Yang, Y. Fan, Study of SiO_2 coat preparation and its anti-coking behaviour, Mater. Res. Innov. 18 (S2) (2014) 527–531.
[9] M. Vardelle, A. Vardelle, P. Fauchais, Spray parameters and particle behavior relationships during plasma spraying, J. Therm. Spray Technol. 2 (1) (1993) 79–91.
[10] B. Pateyron, 'Jets&Poudres' and 'T&Twinner' free download from: ⟨http://www.unilim.fr/spcts⟩.
[11] N. Venkatramani, Industrial plasma torch and application, Curr. Sci. 83 (3) (2002) 254–262.
[12] S. Dresvin, S.U. Mikhailov, Heat exchange of spherical stationary model and small particles moving in a plasma jet, ICHMT, in: P. Fauchais (Ed.), Proceedings of the International Symposium on 'Heat Mass Transfer under Plasma conditions, 1999.
[13] P. Fauchais, A. Vardelle, B. Dussoubs, Quo vadis thermal spraying, J. Therm. Spray Technol. 10 (1) (2001) 44–66.
[14] E. Pfender, Y.C. Lee, Particle dynamics and particle heat and mass transfer in thermal plasmas. Part I. The motion of a single particle without thermal effects, Plasma Chem. Plasma Process. 5 (3) (1985) 211–237.
[15] R. Djebali, Simulation and Modeling of Multiphases and Multicomponents Media Based Lattice Boltzmann Approach (in French) (Ph.D. thesis in co-supervision), Univ. Tunis el Manar & Univ. Limoges, 2011, 112–116.
[16] P.C. Huang, J. Heberlein, E. Pfender, Particle behavior in a two-fluid turbulent plasma jet, Surf. Coat. Technol. 73 (3) (1995) 142–151.
[17] A. Renoux, D. Boulaud, Physique des Aérosols: Partie 1, Techniques de l'Ingénieur, AF 3612.
[18] L. Talbot, R.K. Cheng, R.W. Schefer, D.R. Willis, Thermophoresis of particles in a heated boundary layer, J. Fluid Mech. 101 (4) (1980) 737–758.
19] G. Delluc, G. Mariaux, A. Vardelle, P. Fauchais, B. Pateyron, A numerical tool for plasma spraying. Part I: modelling of plasma jet and particle behaviour, in: R. d'Agostino, P. Favia, F. Fracassi, F. Palumbo (Eds.), Proceedings of the 16th ISPC Taormina, University of Bari, Italy, June 22–27, 2003, 6 pp.
[20] S. Kotowski, J. Sieniawski, M. Góral, Modelling and simulation of plasma spraying process with a use of Jets&Poudres program, J. Achiev. Mater. Manuf. Eng. 55/2 (2012) 547–550.
[21] G. Delluc, L. Perrin, H. Ageorges, P. Fauchais, B. Pateyron, Modelling of plasma jet and particle behaviour in spraying cond itions. Thermal Spray 2004: Advances in Technology and Application: Proceedings of the International Thermal Spray Conference, Osaka, Japan, 10–12 May, 2004.
[22] Y.P. Wan, V. Gupta, Q. Deng, S. Sampath, V. Prasad, Modeling and visualization of plasma spraying of functionally graded materials and its application to the optimization of spray conditions, J. Therm. Spray Technol. 10 (2) (2001) 382–389.
[23] W. Smith, T.J. Jewett, S. Sampath, W.D. Swank, J.R. Fincke, Thermal Spray: A United Forum for Scientific and Technological Advances, in: C.C. Berndt (Ed.), ASM International, Materials Park, OH, 1997, pp. 607–612.